



LIGHTWEIGHT STRUCTURES in CIVIL ENGINEERING

CONTEMPORARY PROBLEMS

Monograph from Scientific Seminar

Organized by Polish Chapters of

International Association for Shell and Spatial Structures

Lodz University of Technology

Faculty of Civil Engineering, Architecture and Environmental

Engineering

XXIV LSCE

Lódź, 7th of December 2018 (Friday)



APPLICATION OF HYPERELASTIC MATERIAL MODELS IN LARGE STRAINS STABILITY ANALYSIS OF SHELL STRUCTURES

S. Jemioło ¹⁾ A. Franus ²⁾

¹⁾ Prof., Faculty of Civil Engineering, Warsaw University of Technology, POLAND, s.jemioło@il.pw.edu.pl

²⁾ MSc, Faculty of Civil Engineering, Warsaw University of Technology, POLAND, a.franus@il.pw.edu.pl

ABSTRACT: The present study addresses an application of the Mooney-Rivlin and Blatz-Ko material models in stability analysis of shell structures. These models are suitable for large deformations as well as finite rotations. The constitutive relations are implemented in the finite element software ABAQUS/Standard 6.14. To this end, UHYPER user subroutine is employed, which is dedicated for isotropic models. The procedure allows to solve a boundary value problem involving either shell or spatial finite elements. Solutions of presented exemplary problems are obtained on the basis of the Riks algorithm. In order to compare results, 3D and 2D finite elements models for each one are considered. Moreover, calculations are performed in the case of widely used “standard nonlinear analysis”, which is not consistent with a formulation based on large strains hyperelasticity.

Keywords: hyperelasticity, polyconvex stored-energy function, stability analysis, large strains

1. INTRODUCTION

The present study addresses an application of the theory of hyperelasticity (Ref.1, 2) and finite element software ABAQUS/Standard 6.14 (Ref. 3, 4) in stability analysis of shell structures (Ref. 5-8). Three constitutive models of isotropic incompressible (model MR, Ref. 2) and compressible nonlinear elastic materials (model NL (Ref. 2) and model BK (Ref. 9)) are used (Ref. 1, 2). MR and NL models are available in ABAQUS’s material models library (Ref. 3,4). One of the objective of this paper is the numerical implementation of the BK model in ABAQUS/Standard 6.14 finite element program (Ref. 3,4). The program has interfaces that allow the user to implement their own material models. In the special case of the hyperelastic isotropic materials it is required only to write a Fortran code of the stored energy function with its derivatives with respect to the strain invariants in the form of UHYPER subroutine.

2. LARGE STRAINS HYPERELASTICITY

An elastic material is called hyperelastic, cf. (Ref. 1), if there exists a stored energy function $W(\mathbf{F})$, ($\mathbf{F} \in Lin^+$, $\dim Lin^+ = 9$), such that

$$\mathbf{S} = \frac{\partial W(\mathbf{F})}{\partial \mathbf{F}}, \quad (1)$$

where \mathbf{S} is the first Piola-Kirchhoff stress tensor and \mathbf{F} defines a “deformation gradient” as $\mathbf{F} = \partial \chi(\mathbf{X}, t) / \partial \mathbf{X}$. The function $\chi(\mathbf{X}, t)$ defines an actual configuration of the body with respect to an initial one, i.e. $\mathbf{x} = \chi(\mathbf{X}, t)$. Since $J = \det \mathbf{F} > 0$, the mapping χ is oriented-preserving and locally invertible. The polar decomposition states $\mathbf{F} = \mathbf{R}\mathbf{U} = \mathbf{V}\mathbf{R}$, which means that any \mathbf{F} can be multiplicatively decomposed into a rotation tensor $\mathbf{R} \in SO(3)$ (Ref. 1) and so called the right $\mathbf{U} = \sqrt{\mathbf{F}^T \mathbf{F}} = \sqrt{\mathbf{C}}$ or the left $\mathbf{V} = \sqrt{\mathbf{F}\mathbf{F}^T} = \sqrt{\mathbf{B}}$ stretch tensor (Ref. 1), ($\mathbf{U}, \mathbf{V} \in Sym^+$, $\dim Sym^+ = 6$).

In order to avoid interpenetration of matter, it is necessary to put some restrictions on $W(\mathbf{F})$, see [1,2]:

$$W(\mathbf{F}) \rightarrow +\infty \text{ as } J \rightarrow 0^+, \quad W(\mathbf{F}) \rightarrow +\infty \text{ as } \|\mathbf{F}\| \rightarrow +\infty. \quad (2)$$

We make the assumption that stored-energy function is isotropic, i.e.

$$W(\mathbf{F}) = \tilde{W}(\mathbf{C}) = \tilde{W}(\mathbf{B}) = \tilde{W}(I_1, I_2, I_3), \quad (3)$$

where $I_1 = \text{tr } \mathbf{C} = \text{tr } \mathbf{B}$, $I_2 = \text{tr cof } \mathbf{C} = \text{tr cof } \mathbf{B}$ and $I_3 = J^2$ are the invariants of each of the left and right Cauchy-Green deformation tensors \mathbf{C} and \mathbf{B} (Ref. 1). Then, there exists a solution for a wide class of boundary values problems associated with hyperelastic model when W has the form $W(\mathbf{F}) = W(\mathbf{F}, \text{cof } \mathbf{F}, \det \mathbf{F})$ for some convex W .

Such functions are said to be polyconvex, cf. (Ref. 1). We emphasize that $\mathbf{F}, \text{cof } \mathbf{F}, \det \mathbf{F}$ are connected with the deformation of lines, surface and volume of the body, respectively.

In the case of incompressibility, i.e. $\det \mathbf{F} = 1$, $W(\bar{\mathbf{F}})$ is polyconvex if there exists an extension of the function to convex one $W(\mathbf{F}, \text{cof } \mathbf{F})$ with respect to \mathbf{F} and $\text{cof } \mathbf{F}$, cf. (Ref. 1), such that $W(\bar{\mathbf{F}}) = W(\mathbf{F}, \text{cof } \mathbf{F})$ ($\bar{\mathbf{F}} = J^{-1/3} \mathbf{F}$).

Since \mathbf{S} is non-symmetric, it is convenient to introduce the second Piola-Kirchhoff stress tensor

$$\begin{aligned} \mathbf{T} &= \left. \frac{\partial \tilde{W}(\mathbf{E})}{\partial \mathbf{E}} \right|_{\mathbf{E}=\mathbf{E}^T} = 2 \left. \frac{\partial \tilde{W}(\mathbf{C})}{\partial \mathbf{C}} \right|_{\mathbf{C}=\mathbf{C}^T} = 2(\gamma_1 \mathbf{I} + \gamma_2 \mathbf{C} + \gamma_3 \mathbf{C}^2), \\ \gamma_1 &= \frac{\partial \tilde{W}}{\partial I_1} + \frac{\partial \tilde{W}}{\partial I_2} I_1 + \frac{\partial \tilde{W}}{\partial I_3} I_2, \quad \gamma_2 = -\left(\frac{\partial \tilde{W}}{\partial I_2} + \frac{\partial \tilde{W}}{\partial I_3} I_1 \right), \quad \gamma_3 = \frac{\partial \tilde{W}}{\partial I_3}. \end{aligned} \quad (4)$$

The relationship between the Cauchy stress tensor $\boldsymbol{\sigma}$, the first and second Piola-Kirchhoff ones, namely $J\boldsymbol{\sigma} = \mathbf{S}\mathbf{F}^T = \mathbf{F}\mathbf{T}\mathbf{F}^T$, cf. (Ref. 1, 2), implies a constitutive relation in the spatial description such that

$$\boldsymbol{\sigma} = 2 \frac{\partial \tilde{W}(\mathbf{B})}{\partial \mathbf{B}} \Big|_{\mathbf{B}=\mathbf{B}^T} = \frac{2}{J} (\beta_1 \mathbf{I} + \beta_2 \mathbf{B} + \beta_3 \mathbf{B}^2), \quad (5)$$

$$\beta_1 = \frac{\partial \tilde{W}}{\partial I_3}, \quad \beta_2 = \frac{\partial \tilde{W}}{\partial I_1} + \frac{\partial \tilde{W}}{\partial I_2}, \quad \beta_3 = -\frac{\partial \tilde{W}}{\partial I_2}.$$

The Kirchhoff stress tensor $\boldsymbol{\tau} = J\boldsymbol{\sigma}$ (Ref. 2, 6) is work conjugated to the symmetric rate of deformation tensor $\mathbf{D} = \text{sym}(\dot{\mathbf{F}}\mathbf{F}^{-1})$ with respect to the initial volume so that (Ref. 1)

$$\dot{W} = J\boldsymbol{\sigma} \cdot \mathbf{D} = \boldsymbol{\tau} \cdot \mathbf{D} = \mathbf{S} \cdot \dot{\mathbf{F}} = \mathbf{T} \cdot \dot{\mathbf{E}}, \quad (6)$$

where $\mathbf{E} = (\mathbf{C} - \mathbf{I})/2$ denotes the Lagrangian strain tensor.

In order to implement a hyperelastic material model using UMAT (Ref. 3, 4), corresponding constructive equations needs to define in a rate form. To do so, it is convenient to define a symmetric fourth-order tensor as

$$\bar{\mathcal{C}} = \frac{\partial^2 \tilde{W}(\mathbf{E})}{\partial \mathbf{E} \otimes \partial \mathbf{E}} \Big|_{\mathbf{E}=\mathbf{E}^T} = 4 \frac{\partial^2 \tilde{W}(\mathbf{C})}{\partial \mathbf{C} \otimes \partial \mathbf{C}} \Big|_{\mathbf{C}=\mathbf{C}^T}, \quad (7)$$

which is known as the material (Lagrangian) elasticity tensor, cf. (Ref. 6). It is conjugated to the second Piola-Kirchhoff stress tensor as $\dot{\mathbf{T}} = \bar{\mathcal{C}} \cdot \dot{\mathbf{E}}$. Since we are interested in a spatial description, the push forward is applied to give the Eulerian elasticity tensor (Ref. 6). Finally, the Zaremba- Jaumann rate of the Kirchhoff stress is given by (Ref. 6)

$$\overset{\circ}{\boldsymbol{\tau}} = \mathbf{D}\boldsymbol{\tau} + \mathbf{F}\dot{\mathbf{T}}\mathbf{F}^T + \boldsymbol{\tau}\mathbf{D} = (\mathbf{I}\overset{\circ}{\boldsymbol{\tau}} + \boldsymbol{\tau}\mathbf{I} + \bar{\mathcal{C}}) \cdot \mathbf{D} = \mathcal{C} \cdot \mathbf{D}. \quad (8)$$

3. MATERIAL MODELS

3.1 Constitutive relations

In the case of "standard nonlinear analysis" of elastic structures (option NLGEOM) in the finite element software ABAQUS/Standard (Ref. 3,4) the following constitutive relationships is used (model NL):

$$\boldsymbol{\sigma} = \lambda (\ln J) \mathbf{I} + 2\mu \ln \mathbf{V}, \quad (9)$$

where λ and μ are Lamé elastic constants. It is worth noting that the NL model does not describe hyperelastic behavior of materials which leads to unrealistic results of numerical simulations in the construction areas where significant shear occurs (Ref. 2). Therefore, two hyperelastic models are used in this work. In the case of compressible materials, the model Blatz-Ko (BL) (Ref. 9) is used, whereas for incompressible materials, the Mooney-Rivlin (MR) (Ref. 1, 2) model is used.

The stored energy function of BL model is defined by

$$W = \frac{cb}{2} \left[I_1 - 3 + \frac{1}{a} \left(J^{-2a} - 1 \right) \right] + \frac{c}{2} (1-b) \left[I_2 J^{-2} - 3 + \frac{1}{a} \left(J^{-a} - 1 \right) \right], \quad (10)$$

where $c = \mu, a = \frac{\nu}{1-2\nu}$ and $b \in (0,1]$.

If $J=1$, then from Eq. (10) the well know Mooney-Rivlin energy function is recovered, cf. (Ref. 2). MR and NL models are available in ABAQUS's material models library.

3.2 UHYPER user subroutine

The ABAQUS /Standard FEM software offers possibilities to implement our own material model, see Ref. 4, 10, 11.

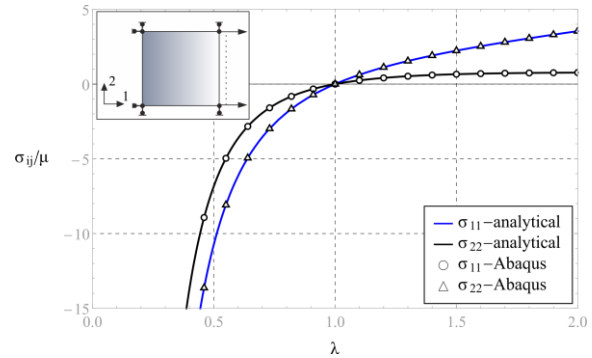


Fig. 1 Components of the Cauchy stress tensor – BK model ($\nu = 0.3$)

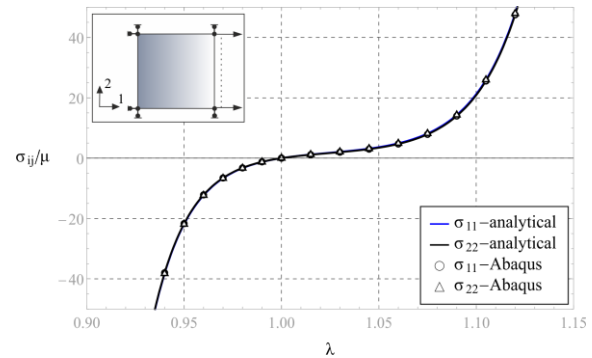


Fig. 2 Components of the Cauchy stress tensor – BK model ($\nu = 0.49$)

One way is to employ user subroutine UHYPER, which can be used to define an isotropic model. It requires that the stored-energy function and its derivatives are defined with respect to the invariants of the form

$$W = \hat{W}(\mathbf{B}) = U(\bar{I}_1, \bar{I}_2, J), \quad (11)$$

$$\bar{I}_1 = \text{tr} \bar{\mathbf{B}}, \quad \bar{I}_2 = \frac{1}{2} (\bar{I}_1^2 - \text{tr} \bar{\mathbf{B}}^2), \quad J = \det \mathbf{F},$$

with $\bar{\mathbf{B}} = \bar{\mathbf{F}}\bar{\mathbf{F}}^T$.

The implementation of the Blatz-Ko (BK) model is verified in simple tests with homogeneous deformations using 3D and 2D elements, as well. The results are compared with the values obtained on the basis of analytical formulas. Plots of the Cauchy stress tensor components and corresponding results obtained on the basis of the UHYPER subroutine in the case of uniaxial deformation are presented in Fig.1 and Fig.2

4. EXAMPLES

As an exemplary boundary value problem a thin-walled circular tube with characteristic dimensions: height $h = 10r$, internal radius $r_w = 0.995r$, external radius $r_e = 1.005r$ with $r = 1[\text{m}]$ under axial compression is considered. A circular cutout located in the central part of the element is introduced to induce relatively large deformations (Ref. 10, 12). In order to compare results, two numerical models are built using respectively: solid elements (3 elements by thickness) of type C3D8R and shell elements of type S4R with linear interpolation functions, see Ref. 4. The loading is realized by displacement control. Thus, following boundary conditions are applied: $u_1 = u_2 = u_3 = 0$ at one end and $u_1 = u_2 = 0, u_3 = -2r$ at the other one according to the coordinate system as in Fig. 3. Solutions are obtained on the basis of the Riks algorithm known from efficiency of solving these types of problems.



Fig. 3 Finite element mesh and cross section of the tube

The Fig. 4 presents plots of averaged stress $\bar{\sigma}$ at the loaded end of the tube as a function of displacement for the incompressible Mooney-Rivlin model. Final deformations of the body corresponding to marked points on equilibrium paths are shown in the figure.

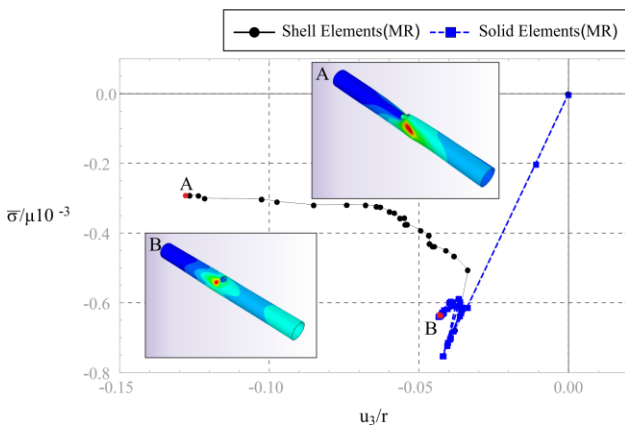


Fig. 4 Plots of averaged stress - MR model with $\theta = 0.9$

The main difference between these two results is a range of the displacement load obtained during the process. In the case of the shell model, computations are carried out up to $u_3 \approx -0.13r$, while for the solid model the extreme displacement value is $u_3 \approx -0.04r$. As expected the second one occurs stiffer. Even though hybrid formulation with reduced integration is applied, a volumetric locking evidently appears, cf. (Ref. 1-3). In both cases, the local form of buckling is observed, followed by a very rapid reduction of the stiffness of the tube. Values of parameters $\nu = 0.3, \theta = 0.9$ are more accurate for models of metallic materials. In the case, numerical tasks are significantly worse posed and solver fails after reaching critical point, see Fig.6 and 8.

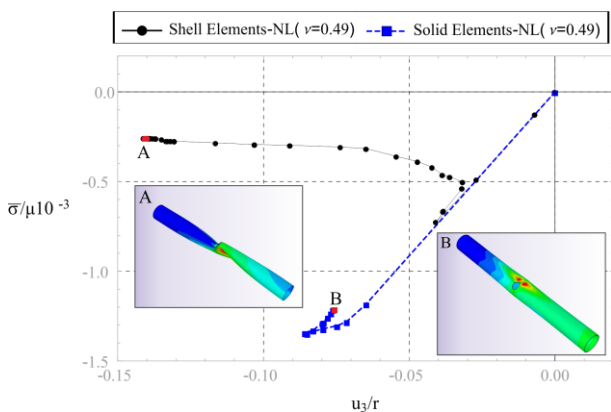


Fig. 5 Plots of averaged stress - NL model with $\nu = 0.49, \theta = 0.9$

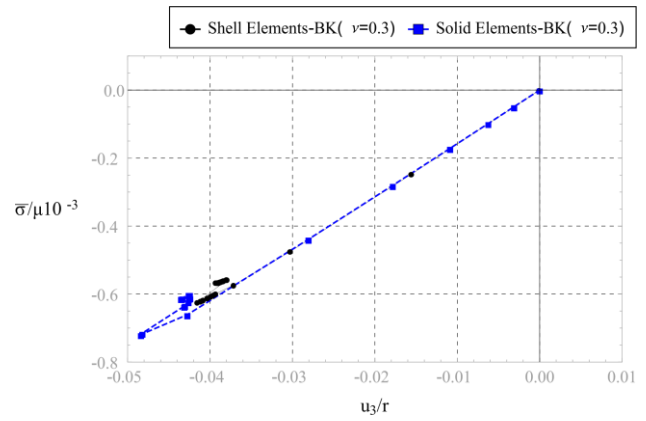


Fig. 6 Plots of averaged stress - BK model with $\nu = 0.3, \theta = 0.9$

Similarly to the MR, in the case of BK and NL compressible models values of critical stresses are higher for solid elements. Difference of these values, see Fig. 5, for NL model is unacceptable. It shows that the solution is very sensitive to values of initial parameters of the Riks procedure. The model is not consistent with a formulation based on large strains hyperelasticity and certainly should not be used in this context.

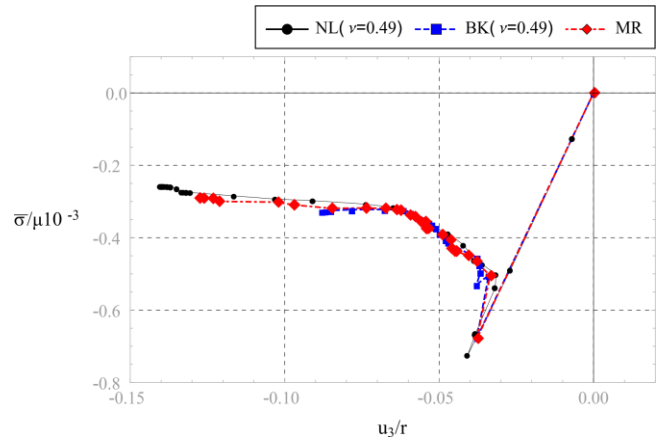


Fig. 7 Comparison of NL, BK and MR materials – shell elements

The NL and BK models with $\nu = 0.49, \theta = 0.9$ represents an almost incompressible material. As shown in Fig. 7, obtained values of critical stresses are very similar in the case of shell elements. Ranges of the displacement load do not differ significantly for NL and MR models. In all cases, the local form of buckling is observed, followed by a very rapid reduction of the stiffness of the tube. Final deformations are shown in the Fig. 9-11 for these three cases.

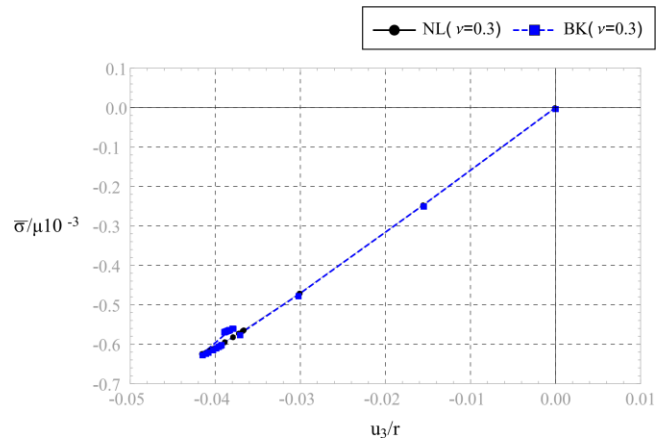


Fig. 8 Comparison of NL and BK materials – shell elements, $\nu = 0.49$

